Level structure of ^{69}Se

I. Stefanescu,[1,2] J. Eberth,[1] G. de Angelis,[3] N. Warr,[1] G. Gersch,[1] T. Steinhardt,[1] O. Thelen,[1] D. Weisshaar,[1] T. Martinez,[3] A. Jungclaus,[4] R. Schwengner,[5] K. P. Lieb,[6] E. A. Stefanova,[6] D. Curien,[7] and A. Gelberg[1]

[1]*Institut für Kernphysik, Universität zu Köln, Zülpicher Strasse 77, D-50937 Köln, Germany*

[2]*Horia-Hulubei National Institute for Physics and Nuclear Engineering, P. O. Box MG-6, Bucharest, Romania*

[3]*Istituto Nazionale di Fisica Nucleare, Laboratori Nazionali de Legnaro, via Romea 4, I-35020 Legnaro, Italy*

[4]*Instituto de Estructura de la Materia, Consejo Superior de Investigaciones Cientificas, E-28006 Madrid, Spain and Departamento de Fisica Teórica, Univ. Autonoma de Madrid, E-28049 Madrid, Spain*

[5]*Institut für Kern- und Hadronenphysik, Forschungszentrum Rossendorf, D-01314 Dresden, Germany*

[6]*II Physikalisches Institut, Universität Göttingen, D-37073 Göttingen, Germany*

[7]*Institut de Recherches Subatomiques, CNRS-IN2P3, F-67037 Strasbourg, France*

(Received 11 September 2003; published 29 March 2004)

Excited levels in ^{69}Se have been studied using the ^{40}Ca(^{32}S,$2pn$)^{69}Se reaction at 95- and 105-MeV beam energy. γ rays have been detected with the EUROBALL spectrometer operated in conjunction with the neutron wall and the charged-particle detector array EUCLIDES. New level sequences with positive and negative parities have been identified from n-$\gamma\gamma$ and n-$\gamma\gamma\gamma$ coincidences. Spins have been assigned to many of the levels on the basis of angular distribution and directional correlation measurements. Excitation energies of the positive-parity yrast band and the branching ratios of its decay are compared with the predictions of the rigid triaxial rotor plus particle model.

DOI: 10.1103/PhysRevC.69.034333 PACS number(s): 23.20.Lv, 21.10.Re, 27.50.+e, 21.60.−n

I. INTRODUCTION

Neutron deficient nuclei with $A\sim 70$ and $N\approx Z$ show a very complex structure. Large prolate and oblate deformations and prolate-oblate shape coexistence at low spin occur in this mass region [1–5]. As both protons and neutrons are simultaneously filling the same levels, the residual interaction between neutrons and protons is significant and polarizing effects may be strong. In the odd-A nuclei, positive-parity bands are generated by the $g_{9/2}$ intruder orbital and have different structures, depending on the nucleon number and deformation. The fact that the $g_{9/2}$ intruder orbital has a relatively high spin introduces important additional effects in the structure of nuclei in this region such as aligned configurations involving two or more quasiparticles and octupole deformations. All these aspects make the $A\sim 70$ mass region a favorite testing ground for different theoretical approaches [6–8].

The shape-coexistence phenomenon in this mass region was first observed in ^{72}Se [9]. The results of the investigations on the even-mass Br, Se, and Kr isotopes and, more recently, on the ^{68}Se nucleus [10,11] have shown that the coexistence of two nuclear shapes is a general feature of the $A\sim 70$ mass region. The study of their odd neighbors completes the information on their structural properties and can be helpful in understanding the effects produced by the coupling of an odd particle to an even-even core with a complex structure and may give more insight into the interplay between oblate and prolate shapes.

Recently reported experimental results concerning the structure of the even-even ^{68}Se nucleus confirmed the fact that the oblate $g_{9/2}$ band in ^{69}Se is generated by coupling the odd neutron to ^{68}Se which is also oblate in the ground state. The oblate ground-state band in ^{68}Se was found to mix strongly with the excited band whose characteristics are consistent with a prolate structure [10–12]. The observation of a systematic decrease of the $B(E2)$ values along the yrast band in ^{70}Se was interpreted as due to the destructive interference of two collective structures at low spin, possibly associated with a change from oblate to prolate deformation [13]. Strong polarization effects are expected to occur by coupling the odd neutron.

The aim of the present investigations is to extend the available information on excited states in ^{69}Se through heavy ion induced reactions. Within the limits of the statistics offered by the present experiments, based on angular distribution and correlation techniques, we assigned the spins to most of the excited levels and extracted the mixing ratios for some intense transitions. Special attention has been paid to the investigation of the $g_{9/2}$ band. The study of the positive-parity nonyrast states constituted another reason for performing the present work because it can offer us important information concerning shape coexistence at low spin.

A detailed analysis of the observed properties of the low-lying positive-parity states has been performed within the rigid triaxial rotor plus particle (RTRP) model of Larsson *et al.* [14].

II. PREVIOUS WORKS

The first spectroscopic information about ^{69}Se was given by the study of its β^+ decay ($T_{1/2}=27.4$ s) to the known low-lying levels of ^{69}As [15]. Within that work, a negative-parity ground state had been established. The low-lying excited states were reported later by two different groups whose in-beam results were partially consistent [3,16]. In Ref. [16], information about the $g_{9/2}$ isomeric state ($T_{1/2}=853\pm 78$ ns) was compared to the properties of the $9/2^+$ states in the $N=35$ isotones and systematic trends concerning

the level structures at low energy and the electromagnetic properties of the γ transitions between these levels were discussed. A detailed study of Wiosna *et al.* [3] established a $g_{9/2}$ band showing a strong-coupling-like pattern. With the Fermi level lying at the beginning of the $g_{9/2}$ orbital, the observed pattern can only occur if the odd-neutron occupies the $K^{\pi}=9/2^{+}$ [404] Nilsson orbit at an oblate deformation. The associated oblate shape was established by the large positive mixing ratio of the lowest member of the yrast band, the 676-keV transition. The work of Arrison *et al.* [17] tried to solve the discrepancy between the two previous studies with respect to the lifetime of the isomeric $9/2^{+}$ level. It provided a conclusive identification of ^{69}Se and confirmed the experimental evidence found by Wiosna *et al.* concerning the major change in the yrast structure compared to other odd-neutron isotopes in the $A\sim 70$ mass region. The single-particle level structure of negative parity below the $9/2^{+}$ isomer was investigated by Pohl *et al.* [18]. The half-life $T_{1/2}=2.0\pm 0.2$ μs of the first excited negative-parity state has been measured, which, together with the internal conversion coefficient of the γ ray deexciting this level, strongly favored a spin and parity assignment of $1/2^{-}$ for the ^{69}Se ground state.

High-spin results were recently reported by Jenkins *et al.* [19]. They extended the previously known $K^{\pi}=9/2^{+}$ oblate band and found that this band is rapidly crossed by a prolate configuration that continues to high spin.

III. EXPERIMENTAL DETAILS AND DATA ANALYSIS

In the present work, the states in ^{69}Se were populated via the ^{40}Ca(^{32}S,$2pn$) reaction at 95- and 105-MeV beam energy delivered by the VIVITRON accelerator of the IReS Strasbourg. In the experiment at 105 MeV, the target consisted of a 860 μg/cm^2 self-supporting foil of enriched 99.965% ^{40}Ca and a foil of 1 mg/cm^2 of enriched 99.9% ^{40}Ca evaporated onto a 15 mg/cm^2 gold backing has been used in the second experiment, performed at 95-MeV beam energy. γ rays were detected with the EUROBALL array [20,21] consisting of 15 Cluster [22] and 26 Clover [23] composite Gedetectors surrounded by a BGO shield providing escape suppression. Charged particles were detected using the 4π device EUCLIDES [24], composed of 40 $\Delta E-E$ silicon telescopes with the five forward elements electrically segmented into four parts. The evaporated neutrons were detected with the Neutron Wall [25], consisting of 50 liquid scintillators covering the forward 1π section of EUROBALL. The trigger conditions in the two experiments were defined by a minimum of two Compton-suppressed Ge detectors fired in coincidence with one neutron in the Neutron Wall. The data from the experiment performed at 105-MeV beam energy were also acquired if a minimum of three Compton-suppressed Ge detectors fired in coincidence with one signal in the Neutron Wall.

Due to the different thickness of the targets and beam energies, ^{69}Se has been populated in the two experiments with different cross sections and at different spins and excitation energies. CASCADE [26] calculations predict that $\approx$3% of the total cross section belongs to the $2pn$, ^{69}Se channel at 95-MeV beam energy and about 1% of the total cross section at 105-MeV beam energy. The reaction at 105 MeV populated the nucleus at high spin and allowed the bands to be extended further. The reaction at 95 MeV using the 1mg/cm^2 backed ^{40}Ca target was useful in the investigation of the nonyrast states of lower spins.

Data were stored on tapes and sorted off-line into $E_\gamma-E_\gamma$ matrices and $E_\gamma-E_\gamma-E_\gamma$ cubes, with particle gates of one or two protons and one neutron in order to enhance the ^{69}Se reaction channel. For energy and efficiency calibrations, ^{152}Eu and ^{56}Co sources were used. A comparison of the peak positions at different detector angles yielded an average velocity of the recoiling nuclei $v/c=2.67\%$. With this value, a Doppler correction of the γ-ray energies was carried out on an event-by-event basis for the data from the self-supporting target experiment. The n-$\gamma\gamma\gamma$ cubes consist of about 10^7 events with a multiplicity greater than 2 in both experiments. The cubes and the matrices were analyzed using the GASPWARE [27] and RADWARE [28] software packages.

An analysis of the directional correlations from oriented states (DCO) was performed to assign the multipole order to the newly observed states. Since the DCO ratios are very sensitive to the observation angles of the coincident γ rays, specific groups of detectors have to be chosen for the analysis. The segmented structure of the EUROBALL detectors leads to the formation of 13 rings positioned at angles of 72°, 81°, 99°, 107°, 123°, 129°, 133°, 137°, 141°, 146°, 149°, 156°, and 163°. For the present DCO analysis, the coincidence data were added up for the four most backward-angle rings (164°, 156°, 149°, and 146°), resulting in a quasiring at a weighted angle of 155° to the beam axis and the four rings near 90° (72°, 81°, 99°, and 107°). A 155° versus 90° γ-γ matrix was created in coincidence with one neutron for each experiment. From these matrices, we extracted the DCO ratios defined as [29]

$$R_{DCO}^{exp}=\frac{I^{\gamma 2}_{155^\circ}(\mathrm{Gate}^{\gamma 1}_{90^\circ})}{I^{\gamma 2}_{90^\circ}(\mathrm{Gate}^{\gamma 1}_{155^\circ})}, \tag{1}$$

where $I^{\gamma 2}_{155^\circ}(\mathrm{Gate}^{\gamma 1}_{90^\circ})$ denotes the efficiency-corrected coincidence intensity of the γ_2 transition observed at 155° when gating on the γ_1 transition observed at 90°. In this geometry, if one gates on a stretched quadrupole transition, the theoretical DCO ratios are $\sim$1 for stretched quadrupole transitions and $\sim$0.5 for pure dipole transitions. If, in contrast, gates are set on a pure dipole transition, the extracted DCO ratios are $\sim$2 for pure quadrupole transitions and $\sim$1 for pure dipole transitions.

Particle-gated angular distributions were analyzed in order to extract the multipole mixing ratios of the γ-rays in ^{69}Se. The data from the experiment at 105 MeV acquired in coincidence with one neutron were sorted into spectra for each of the rings of EUROBALL. To increase the statistics, the resulting spectra of the neighboring rings were added up and the angular distributions were fitted for five points corresponding to the weighted angles of 156° (from the rings at 149°, 156°, and 163°), 139° (rings at 137°, 141°, and 146°), 128° (rings at 123°, 129°, and 133°), 99° (rings at 81° and 99°), and 72° (rings at 72° and 107°). Angular distributions

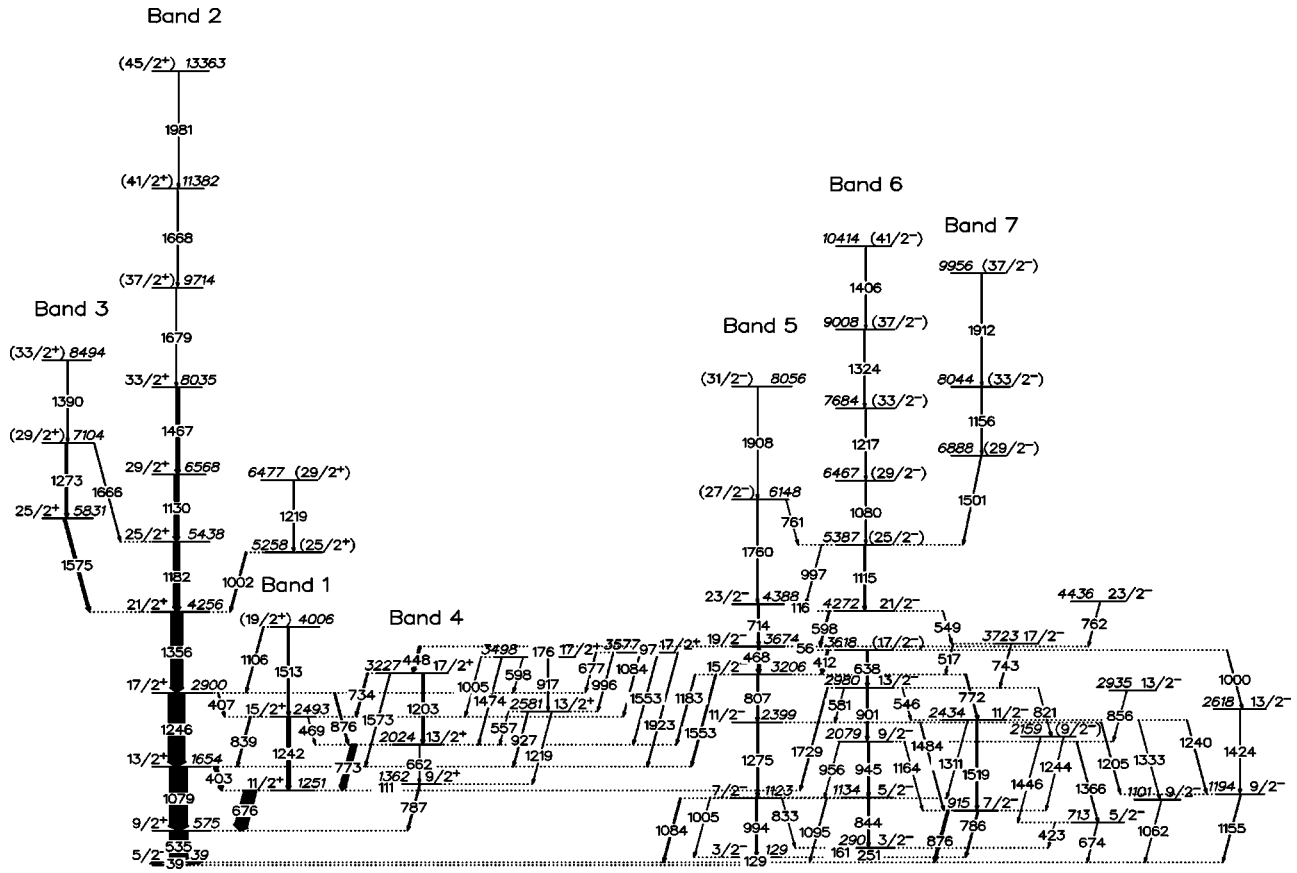

FIG. 1. Level scheme of ^{69}Se obtained from the present work. The widths of the arrows are proportional to the γ-ray intensities. The ground state has the spin and parity $1/2^-$.

for some intense stretched transitions with known angular distribution coefficients were analyzed initially in order to extract the ratio σ/I_i, with σ representing the width of the Gaussian distribution of magnetic substates and I_i being the spin of the initial state. In the analysis, the computer code CHIPLO-2 has been used [30]. A mean value for $\sigma/I_i = 0.35 \pm 0.03$ was found to minimize the χ^2 function and to reproduce the angular distribution coefficients given in the literature [31,32]. This value has been used as a reference value for the final analysis of the angular distribution measurements.

IV. EXPERIMENTAL RESULTS

The current investigations confirm the previously observed yrast transitions and extend the level scheme further. Combining the experimental information obtained from both experiments, new levels were found in both positive- and negative-parity parts of the level scheme. The new levels are arranged in band structures feeding into the yrast bands of the respective parity.

The level scheme shown in Fig. 1 results from the analysis of the data obtained in the present work. The transitions have been placed in the level scheme according to the coincidence relationships and relative intensities. The level scheme is organized into seven different bands labeled from 1 to 7 plus additional single states or structures which cannot be included in rotational-like bands yet. Spin and parities were deduced, whenever possible, from the analysis of the DCO ratios and the angular distribution and from a comparison with the systematics.

The spectroscopic information of the γ rays belonging to ^{69}Se is listed in Table I. The first column gives the energies of the γ transitions obtained from the analysis using the n-$\gamma\gamma$ matrices. The next three columns give their relative intensities, the DCO ratios, and the energy of the gating transition, respectively, extracted from the experiment with the self-supporting target at 105-MeV beam energy. For comparison, the fifth column of the table gives the intensities of the γ rays extracted from the experiment using the gold-backed target and 95-MeV beam energy. In both cases, the intensities are normalized to the intensity of the 733.3-keV transition which is set to be 100. The DCO ratios extracted from the experiment at 95-MeV confirm and successfully complete the information on the multipole order of the γ rays extracted from the experiment at 105-MeV. Finally, the ninth and the tenth columns of Table I give the assigned multipolarities and the corresponding spin sequence, based on the measured DCO ratios and angular distributions.

A. Positive-parity states

Spin and parity of $1/2^-$ have been assigned to the ground state by Pohl *et al.* [18]. The $9/2^+$ isomeric state at 574.6-

TABLE I. Energies, relative intensities, and DCO ratios of γ-ray transitions assigned to ^{69}Se. The intensities are normalized to the 773.3-keV transition, set to be 100.

		105 MeV			95 MeV				
E_{level} (keV)	E_γ (keV)	I_γ	R_{DCO}	Gate	I_γ	R_{DCO}	Gate	σL	$I_i^\pi \rightarrow I_f^\pi$
0.0									$\frac{1}{2}^-$
39.4	39.4[a]							$E2$	$\frac{5}{2}^- \rightarrow \frac{1}{2}^-$
129.1	129.1(2)	23.8(12)			33.2(13)	0.33(7)	468.0	$M1/E2$	$\frac{3}{2}^- \rightarrow \frac{1}{2}^-$
						0.32(3)	807.0		
	90.3(1)	7.1(6)			11.6(8)			$M1/E2$	$\frac{3}{2}^- \rightarrow \frac{5}{2}^-$
290.1	161.3(4)	5.3(4)			24.9(38)	0.51(27)	807.0	$M1$	$\frac{3}{2}^- \rightarrow \frac{3}{2}^-$
	250.7(2)	5.6(18)			29.3(22)	1.53(20)	844.0	$M1/E2$	$\frac{3}{2}^- \rightarrow \frac{5}{2}^-$
574.6	534.5[a]							$E2$	$\frac{9}{2}^+ \rightarrow \frac{5}{2}^-$
713.1	422.6(1)	0.8(1)			3.0(6)	1.06(77)	129.1	$M1/E2$	$\frac{5}{2}^- \rightarrow \frac{3}{2}^-$
	673.7(3)	3.3(4)			11.3(5)			$M1/E2$	$\frac{5}{2}^- \rightarrow \frac{5}{2}^-$
914.6	786.4(5)	17.7(11)			54.4(87)	0.93(18)	807.0	$E2$	$\frac{7}{2}^- \rightarrow \frac{3}{2}^-$
	876.2(4)	35.2(78)			94.8(41)	0.84(14)	807.0	$M1/E2$	$\frac{7}{2}^- \rightarrow \frac{5}{2}^-$
1101.8	1061.7(4)	1.1(4)			4.6(8)	1.53(41)	468.0	$E2$	$\frac{9}{2}^- \rightarrow \frac{5}{2}^-$
1123.5	993.9(2)	19.6(12)			50.0(88)	0.97(18)	468.0	$E2$	$\frac{7}{2}^- \rightarrow \frac{3}{2}^-$
	1084.1(3)	18.1(30)			44.1(41)	0.64(11)	468.0	$M1/E2$	$\frac{7}{2}^- \rightarrow \frac{5}{2}^-$
	833.2(3)	0.7(3)			1.8(3)			$E2$	$\frac{7}{2}^- \rightarrow \frac{3}{2}^-$
1134.7	844.0(4)	3.3(10)			11.2(17)	0.92(31)	129.1	$M1/E2$	$\frac{5}{2}^- \rightarrow \frac{3}{2}^-$
	1004.8(2)	1.1(3)			2.4(5)			$M1/E2$	$\frac{5}{2}^- \rightarrow \frac{3}{2}^-$
	1095.3(5)	3.1(4)			12.5(28)			$M1/E2$	$\frac{5}{2}^- \rightarrow \frac{5}{2}^-$
1193.8	1155.4(2)	8.2(6)			41.7(5)	0.89(16)	807.0	$E2$	$\frac{9}{2}^- \rightarrow \frac{5}{2}^-$
1250.7	675.9(3)	210.8(90)	1.20(13)	1355.7	164.3(74)	0.95(16)	714.2	$M1/E2$	$\frac{11}{2}^+ \rightarrow \frac{9}{2}^+$
1361.8	110.7(2)	3.3(30)			8.0(5)	0.29(8)	675.9	$M1/E2$	$\frac{9}{2}^+ \rightarrow \frac{11}{2}^+$
	787.2(3)	15.3(41)			38.2(47)			$M1/E2$	$\frac{9}{2}^+ \rightarrow \frac{9}{2}^+$
1653.7	403.1(6)	57.0(3)	0.65(6)	675.9	50.9(48)	0.53(10)	675.9	$M1/E2$	$\frac{13}{2}^+ \rightarrow \frac{11}{2}^+$
	1079.1(4)	309.2(110)	1.04(8)	1355.7	154.0(66)			$E2$	$\frac{13}{2}^+ \rightarrow \frac{9}{2}^+$
2023.8	773.3(2)	100			100	1.08(11)	714.2	$M1/E2$	$\frac{13}{2}^+ \rightarrow \frac{11}{2}^+$
	662.3(3)	1.5(5)			3.5(2)			$E2$	$\frac{13}{2}^+ \rightarrow \frac{9}{2}^+$
2079.4	944.7(2)	4.7(4)			12.1(18)	1.83(78)	129.1	$E2$	$\frac{9}{2}^- \rightarrow \frac{5}{2}^-$
						1.47(31)	844.0		
	956.3(1)	1.2(2)			4.4(3)			$M1/E2$	$\frac{9}{2}^- \rightarrow \frac{7}{2}^-$
	1163.8(2)	1.0(2)			3.5(7)			$M1/E2$	$\frac{9}{2}^- \rightarrow \frac{7}{2}^-$
	1366.1(4)	3.2(8)			9.0(17)			$E2$	$\frac{9}{2}^- \rightarrow \frac{5}{2}^-$
2158.9	1244.3(4)	1.0(2)			3.6(7)			$(M1/E2)$	$\left(\frac{9}{2}^-\right) \rightarrow \frac{7}{2}^-$
	1446.2(1)	0.7(4)			1.3(3)			$(E2)$	$\left(\frac{9}{2}^-\right) \rightarrow \frac{5}{2}^-$
2398.6	1205.2(2)	3.6(3)			8.4(21)	0.22(7)	807.0	$M1/E2$	$\frac{11}{2}^+ \rightarrow \frac{9}{2}^-$
	1275.2(3)	12.4(12)			28.7(47)	1.14(15)	468.0	$E2$	$\frac{11}{2}^+ \rightarrow \frac{7}{2}^-$
	1484.0(4)	5.2(5)			12.9(20)	0.93(17)	468.0	$E2$	$\frac{11}{2}^+ \rightarrow \frac{7}{2}^-$
2433.9	1240.3(4)	4.5(11)			13.6(39)	0.57(13)	468.0	$M1/E2$	$\frac{11}{2}^+ \rightarrow \frac{9}{2}^-$
	1311.1(2)	1.9(4)			2.7(5)	1.13(47)	468.0	$E2$	$\frac{11}{2}^+ \rightarrow \frac{7}{2}^-$
	1333.3(4)	0.7(3)			1.3(3)	0.76(30)	468.0	$M1/E2$	$\frac{11}{2}^+ \rightarrow \frac{9}{2}^-$
	1519.3(2)	1.9(2)			11.0(21)	1.05(26)	468.0	$E2$	$\frac{11}{2}^+ \rightarrow \frac{7}{2}^-$

TABLE I. (*Continued.*)

E_{level} (keV)	E_γ (keV)	105 MeV			95 MeV			σL	$I_i^\pi \rightarrow I_f^\pi$
		I_γ	R_{DCO}	Gate	I_γ	R_{DCO}	Gate		
2492.7	469.2(4)	2.7(4)			13.3(18)			$M1/E2$	$\frac{15}{2}^+ \rightarrow \frac{13}{2}^+$
	838.6(2)	6.3(17)	0.69(11)	1079.1	2.2(2)	0.37(14)	675.9	$M1/E2$	$\frac{15}{2}^+ \rightarrow \frac{13}{2}^+$
	1242.2(3)	47.8(34)			26.9(24)	1.11(24)	714.2	$E2$	$\frac{15}{2}^+ \rightarrow \frac{11}{2}^+$
2581.0	557.3(4)	3.1(3)			2.4(2)	0.85(11)	773.3	$M1/E2$	$\frac{13}{2}^+ \rightarrow \frac{13}{2}^+$
	926.8(4)	4.7(2)			2.7(3)	0.81(11)	1079.1	$M1/E2$	$\frac{13}{2}^+ \rightarrow \frac{13}{2}^+$
	1219.2(3)	3.3(7)			1.7(4)			$E2$	$\frac{13}{2}^+ \rightarrow \frac{9}{2}^+$
2618.1	1424.3(4)	5.3(4)			2.9(5)	0.79(14)	1154.4	$E2$	$\frac{13}{2}^+ \rightarrow \frac{9}{2}^-$
2900.0	406.7(5)	4.2(5)			2.1(3)	0.53(21)	1079.1	$M1/E2$	$\frac{17}{2}^+ \rightarrow \frac{15}{2}^+$
	876.2(2)	6.7(8)			2.0(6)			$E2$	$\frac{17}{2}^+ \rightarrow \frac{13}{2}^+$
	1246.3(4)	272.6(114)	0.95(7)	1079.1				$E2$	$\frac{17}{2}^+ \rightarrow \frac{13}{2}^+$
2935.5	856.1(4)	1.4(6)			2.6(5)	1.36(67)	844.1	$E2$	$\frac{13}{2}^+ \rightarrow \frac{9}{2}^-$
2979.6	546.2(5)	<0.1			0.4(2)			$M1/E2$	$\frac{13}{2}^+ \rightarrow \frac{11}{2}^+$
	581.1(3)	1.1(3)			2.6(5)			$M1/E2$	$\frac{13}{2}^+ \rightarrow \frac{11}{2}^+$
	821.1(3)	2.2(2)			3.6(7)			$(M1/E2)$	$\frac{13}{2}^+ \rightarrow (\frac{11}{2}^+)$
	901.2(5)	6.9(6)			15.6(27)	1.37(35)	844.0	$E2$	$\frac{13}{2}^+ \rightarrow \frac{9}{2}^-$
	1729.8(2)	6.7(6)			8.9(6)			$E1$	$\frac{13}{2}^+ \rightarrow \frac{11}{2}^+$
3205.6	807.0(3)	14.9(14)			34.9(58)	1.05(10)	468.0	$E2$	$\frac{15}{2}^+ \rightarrow \frac{11}{2}^+$
	772.3(4)	6.8(5)			13.8(19)	1.06(15)	1154.4	$E2$	$\frac{15}{2}^+ \rightarrow \frac{11}{2}^+$
	1183.2(5)	6.1(3)			13.6(38)	0.59(11)	468.0	$E1$	$\frac{15}{2}^+ \rightarrow \frac{13}{2}^+$
	1553.1(3)	17.2(18)			10.6(7)	0.56(10)	468.0	$E1$	$\frac{15}{2}^+ \rightarrow \frac{13}{2}^+$
3227.1	734.2(21)	18.7(2)	0.68(15)	675.9	8.6(8)	0.8(2)	1079.1	$M1/E2$	$\frac{17}{2}^+ \rightarrow \frac{15}{2}^+$
	1203.3(2)	31.0(19)			14.0(7)	0.91(17)	714.2	$E2$	$\frac{17}{2}^+ \rightarrow \frac{13}{2}^+$
	1573.5(4)	11.7(9)			2.7(11)			$E2$	$\frac{17}{2}^+ \rightarrow \frac{13}{2}^+$
3498.3	598.3(5)	0.8(4)			0.5(3)			$M1/E2$	$\frac{17}{2}^+ \rightarrow \frac{17}{2}^+$
	917.3(4)	2.7(6)			1.4(2)			$E2$	$\frac{17}{2}^+ \rightarrow \frac{13}{2}^+$
	1005.4(2)	0.3(2)			$<0.2(2)$			$M1/E2$	$\frac{17}{2}^+ \rightarrow \frac{15}{2}^+$
	1474.5(4)	7.8(12)			3.8(3)	0.82(17)	773.3	$E2$	$\frac{17}{2}^+ \rightarrow \frac{13}{2}^+$
3576.5	677.2(10)	3.2(1)			3.4(3)	0.36(11)	1079.1	$M1/E2$	$\frac{17}{2}^+ \rightarrow \frac{17}{2}^+$
	996.3(4)	3.5(9)			2.3(2)			$E2$	$\frac{17}{2}^+ \rightarrow \frac{13}{2}^+$
	1083.8(1)	3.1(7)			3.7(3)	1.05(27)	1079.1	$M1/E2$	$\frac{17}{2}^+ \rightarrow \frac{15}{2}^+$
	1553.0(3)	2.1(2)			2.4(1)	0.70(15)	773.3	$E2$	$\frac{17}{2}^+ \rightarrow \frac{13}{2}^+$
	1923.2(4)	3.2(4)			3.2(5)	0.84(26)	1079.1	$E2$	$\frac{17}{2}^+ \rightarrow \frac{13}{2}^+$
3617.6	412.0(2)	7.3(7)	0.59(7)	773.3	9.3(17)	0.52(4)	807.0	$M1/E2$	$\frac{17}{2}^+ \rightarrow \frac{15}{2}^+$
	638.0(2)	3.3(4)			8.4(5)	2.12(56)	129.1	$E2$	$\frac{17}{2}^+ \rightarrow \frac{13}{2}^+$
	1000.1(4)	3.7(5)			9.3(21)	1.18(24)	1154.4	$E2$	$\frac{17}{2}^+ \rightarrow \frac{13}{2}^+$
3673.6	56.2(3)	$\sim 18^b$						$M1/E2$	$\frac{19}{2}^+ \rightarrow \frac{17}{2}^+$
	97.3(3)	2.4(2)			3.1(4)	0.31(8)	714.2	$E1$	$\frac{19}{2}^+ \rightarrow \frac{17}{2}^+$
	176.2(2)	1.4(1)			1.9(1)	0.55(7)	714.4	$E1$	$\frac{19}{2}^+ \rightarrow \frac{17}{2}^+$
	448.2(2)	14.1(12)	0.56(9)	773.3	18.9(11)	0.46(5)	714.2	$E1$	$\frac{19}{2}^+ \rightarrow \frac{17}{2}^+$
	468.0(5)	11.4(9)	0.81(12)	675.9	11.4(9)	0.91(8)	714.2	$E2$	$\frac{19}{2}^+ \rightarrow \frac{15}{2}^+$
3722.7	517.1(5)	3.7(5)			3.2(3)	0.43(12)	1275.2	$M1/E2$	$\frac{17}{2}^+ \rightarrow \frac{15}{2}^+$
	743.3(2)	1.6(3)			0.6(1)			$E2$	$\frac{17}{2}^+ \rightarrow \frac{13}{2}^+$

TABLE I. (*Continued.*)

E_{level} (keV)	E_γ (keV)	105 MeV			95 MeV			σL	$I_i^\pi \rightarrow I_f^\pi$
		I_γ	R_{DCO}	Gate	I_γ	R_{DCO}	Gate		
4006.3	1106.3(4)	<1						$(M1/E2)$	$(\frac{19}{2}^+) \rightarrow \frac{17}{2}^+$
	1512.6(5)	1.6(5)						$(E2)$	$(\frac{19}{2}^+) \rightarrow \frac{15}{2}^+$
4255.7	1355.7(3)	190.7(95)	1.09(9)	1079.1				$E2$	$\frac{21}{2}^+ \rightarrow \frac{17}{2}^+$
4271.8	549.4(4)	1.2(2)			2.7(2)			$E2$	$\frac{21}{2}^+ \rightarrow \frac{17}{2}^+$
	598.2(5)	20.6(14)	0.41(8)	773.3	18.1(10)	0.41(9)	1275.2	$M1/E2$	$\frac{21}{2}^+ \rightarrow \frac{19}{2}^+$
4387.8	116.4(3)	1.8(2)			1.7(11)	0.37(15)	468.0	$M1/E2$	$\frac{23}{2}^+ \rightarrow \frac{21}{2}^+$
	714.2(5)	17.2(18)	1.11(17)	773.3	17.6(13)	1.12(11)	468.0	$E2$	$\frac{23}{2}^+ \rightarrow \frac{19}{2}^+$
4435.7	762.1(3)	8.8(8)			4.0(6)	1.1(2)	468.0	$(E2)$	$\frac{23}{2}^+ \rightarrow \frac{19}{2}^+$
5257.9	1002.2(4)	21.1(7)			6.4(3)			$(E2)$	$(\frac{25}{2}^+) \rightarrow \frac{21}{2}^+$
5386.9	996.8(4)	3.1(4)			1.4(7)			$(M1/E2)$	$(\frac{25}{2}^+) \rightarrow \frac{23}{2}^+$
	1115.1(2)	33.2(21)			3.7(3)			$(E2)$	$(\frac{29}{2}^+) \rightarrow (\frac{25}{2}^+)$
5438.0	1182.3(3)	109.4(65)	1.09(10)	1355.7				$E2$	$\frac{25}{2}^+ \rightarrow \frac{21}{2}^+$
5830.8	1575.1(4)	41.8(34)	1.34(27)	1355.7				$E2$	$\frac{25}{2}^+ \rightarrow \frac{21}{2}^+$
6147.8	761.4(4)	1.7(4)						$(M1/E2)$	$(\frac{27}{2}^+) \rightarrow (\frac{25}{2}^+)$
	1760.0(2)	5.6(21)						$(E2)$	$(\frac{27}{2}^+) \rightarrow \frac{23}{2}^+$
6467.0	1080.1(3)	2.5(11)						$(E2)$	$(\frac{29}{2}^+) \rightarrow (\frac{25}{2}^+)$
6477.2	1219.3(2)	11.9(18)						$(E2)$	$(\frac{29}{2}^+) \rightarrow (\frac{25}{2}^+)$
6568.2	1130.2(3)	72.8(42)	1.12(15)	1079.1				$E2$	$\frac{29}{2}^+ \rightarrow \frac{25}{2}^+$
6887.7	1501.2.3(4)	8.4(27)						$(E2)$	$(\frac{29}{2}^+) \rightarrow (\frac{25}{2}^+)$
7104.3	1273.5(3)	29.9(17)						$(E2)$	$(\frac{29}{2}^+) \rightarrow (\frac{25}{2}^+)$
	1666.2(3)	8.2(5)						$(E2)$	$(\frac{29}{2}^+) \rightarrow \frac{25}{2}^+$
7684.4	1217.4(4)	3.4(11)						$(E2)$	$(\frac{33}{2}^+) \rightarrow (\frac{29}{2}^+)$
8035.0	1466.8(5)	46.2(32)	1.08(15)	1355.7				$(E2)$	$(\frac{33}{2}^+) \rightarrow \frac{29}{2}^+$
8044.3	1156.3(4)	5.1(3)						$(E2)$	$(\frac{33}{2}^+) \rightarrow (\frac{29}{2}^+)$
8056.0	1910.2(4)	1.2(2)						$(E2)$	$(\frac{31}{2}^+) \rightarrow (\frac{27}{2}^+)$
8494.1	1389.8(4)	4.5(14)						$(E2)$	$(\frac{33}{2}^+) \rightarrow (\frac{29}{2}^+)$
9008.1	1323.7(3)	3.2(4)						$(E2)$	$(\frac{37}{2}^+) \rightarrow (\frac{33}{2}^+)$
9714.2	1679.2(4)	9.9(12)						$(E2)$	$(\frac{37}{2}^+) \rightarrow (\frac{33}{2}^+)$
9956.2	1911.9(3)	3.3(7)						$(E2)$	$(\frac{37}{2}^+) \rightarrow (\frac{33}{2}^+)$
10414.4	1406.3(5)	2.7(2)						$(E2)$	$(\frac{41}{2}^+) \rightarrow (\frac{37}{2}^+)$
11382.6	1668.4(7)	7.4(3)						$(E2)$	$(\frac{41}{2}^+) \rightarrow (\frac{37}{2}^+)$
13363.1	1980.5(9)	3.1(11)						$(E2)$	$(\frac{45}{2}^+) \rightarrow (\frac{41}{2}^+)$

[a]From Ref. [58].
[b]From the intensities balance.

keV excitation energy constitutes the bandhead of the positive-parity structures. A strong-coupled-like band, labeled band 1, develops yrast at low excitation energies. In Ref. [19], two $\Delta I=1$ transitions, 838.6 and 406.7 keV, were newly reported, as well as the $\Delta I=2$, 1242.2-keV transition, as being the extension of the previous $9/2^+$-$11/2^+$-$13/2^+$ observed sequence. Our data support this assignment. We propose a new level at 4006.3 keV with spin $(19/2^+)$ as belonging to the oblate yrast band, depopulating by a $\Delta I=2$, 1512-keV γ ray on the 2492.7-keV level and a $\Delta I=1$, 1106.3-keV transition on the 2900.0-keV level. They show a similar degree of signature splitting as the previously known $9/2^+$-$11/2^+$-$13/2^+$-$15/2^+$-$17/2^+$ sequence. Figure 2(a) shows a spectrum double-gated on the 675.9- and 1242.2-keV γ rays in which our extension of the ground-state band can be observed. Although the statistics are low, the double-gating procedure leads to extremely clean spectra.

The fact that the low-spin states were favorably populated in the reaction on the 1 mg/cm^2 ^{40}Ca target at 95 MeV allowed us to identify the second $9/2^+$ state at 1361.8-keV

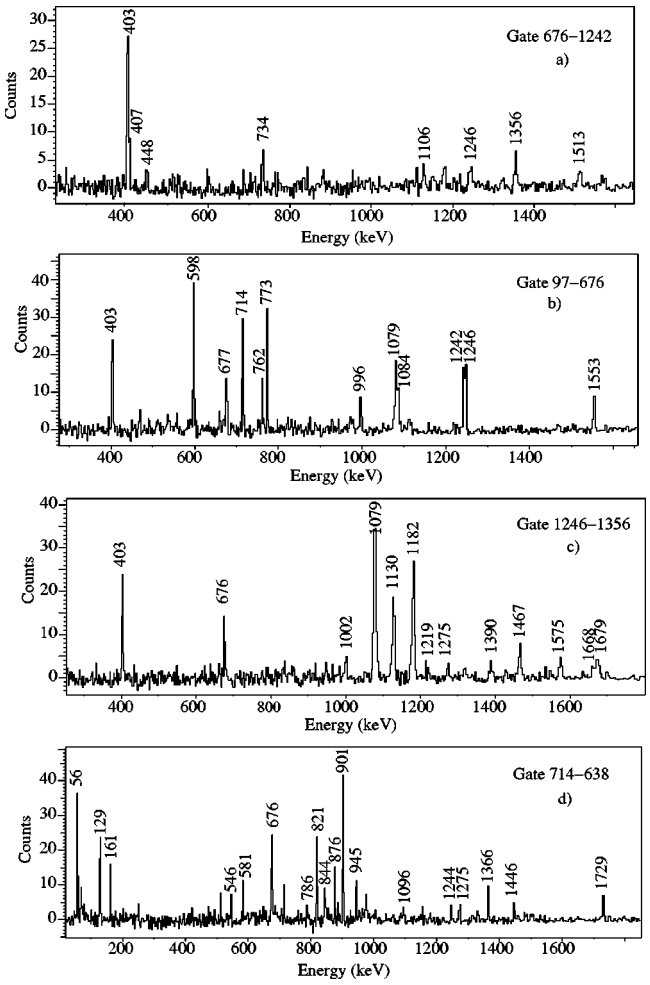

FIG. 2. Examples of doubly gated coincidence spectra from the n-$\gamma\gamma\gamma$ cube. Panels (a) and (b) present spectra acquired from the experiment at 105 MeV using the thin ^{40}Ca target and the panels (c) and (d) contain spectra acquired from the experiment at 95 MeV using a gold-backed ^{40}Ca target. Peaks labeled with their energies in keV are assigned to ^{69}Se.

excitation energy, lying close to the first $11/2^+$ state at 1250.7 keV and which decays to the first $9/2^+$ level by a 787.2-keV transition. Three new levels at 2581.0, 3498.3, and 3576.5 keV were also well populated in the reaction at 95-MeV beam energy. Good statistics allowed us to extract the multipole order of the transitions depopulating these levels supporting the spin assignments of $13/2^+$, $17/2^+$, and $17/2^+$, respectively. Up to now, four levels with spin $17/2^+$ have been found in ^{69}Se. The yrast state at 2900.0-keV excitation energy is only populated by transitions decaying from the higher positive-parity yrast levels. The other three levels—at 3227.1, 3498.3, and 3576.5 keV—are populated by transitions decaying from the negative-parity state with spin $19/2^-$ at 3673.6 keV. In the spectrum from Fig. 2(b) the 996.3-, 1083.8-, 677.2-, and 1553-keV γ rays which deexcite the newly found level at 3576.5 keV can be observed.

In Table II the angular distribution coefficients A_2/A_0 and A_4/A_0 and mixing ratios δ are listed. As an example for the quality of the data, the left side of Fig. 3 shows the angular distributions of the 675.9-$(11/2^+ \rightarrow 9/2^+)$, 773.2-$(13/2^+ \rightarrow 11/2^+)$, and 403.1-keV $(13/2^+ \rightarrow 11/2^+)$ γ rays. Our angular distribution results for the 675.9-keV transition (Fig. 3, top) agree with the two values for the mixing ratios obtained by Jenkins *et al.* [19]. As they pointed out, the smaller value of the mixing ratio fully agrees with the expected value for the quadrupole moment $Q_0 \approx -3$ *e* b when considering an oblate shape and a deformation parameter $\beta_2 \approx -0.3$ in agreement with the theoretical predictions. But the large value of the mixing ratio cannot be excluded because it may explain the quadrupole behavior of the 675.9-keV transition in the angular correlation analysis (see Table I). For example, gating on the 714.2-keV γ ray, which from the angular distribution and correlation data was found to have a quadrupole character, or gating on the stretched quadrupole 1355.7-keV transition, the values obtained for the DCO ratios are 0.95(16) and 1.20(13), respectively, consistent with a $\Delta I = 2$ multipolarity or a large dipole-quadrupole mixing ratio for the 675.9-keV γ ray. The same situation appears in the angular correlation analysis of the 773.3-keV transition. With a gate on the 714.5-keV transition, a DCO value of 1.08(11) is obtained, suggesting a quadrupole character and a spin assignment of $15/2^+$ for the level at 2023.8 keV. In our analysis of the angular distribution data for the 773.3-keV transition, again two solutions are found, one corresponding to a large multipole mixing ratio $\delta = 2.30 \pm 0.39$ and the other to a small multipole mixing ratio $\delta = 0.57^{+0.10}_{-0.07}$ (see Fig. 3 and Table II). The former solution has a reduced $\chi^2 = 0.867$ value whereas the latter has $\chi^2 = 1.245$. No other minima were found in the plot of χ^2 vs δ as represented in Fig. 3. With such a large value of δ for the 773.3-keV transition, we assume a mixed $E2/M1$ character and a spin of $13/2^+$ for the 2023.8-keV level, in agreement with the systematics of the light germanium isotopes [31,33,35]. A spin of $13/2^+$ for the 2023.8-keV level is also consistent with the results of the directional correlations analysis for the 1203.3-, 448.2-, and 1183.2-keV transitions populating the level. The angular distribution of the 403.1-keV transition shows an isotropic character, giving the value $\delta = 0.16 \pm 0.05$ for the mixing ratio (Fig. 3, bottom).

Large values of the mixing ratios for the low members of the yrast band have also been measured in ^{69}Ge [33] and ^{75}Kr [4,34]. A simple prolate-oblate mixing model is proposed in Ref. [4] in order to describe the anomalous behavior of transition probabilities in ^{75}Kr.

At spin $21/2^+$ the oblate structure was found by Jenkins and co-workers to be crossed by a prolate configuration which continues at high spin. Above spin $21/2^+$ additional structures occur. The $25/2^+$ state at 5438.0-keV excitation energy belongs to the prolate configuration found by Jenkins *et al.* [19]. The second $25/2^+$ state is depopulated by the 1575.1-keV transition. In the work of Jenkins *et al.* [19] this state was found to be populated by the 1002.2-keV transition. Our data support the existence of the 1002.2-keV transition but not its placement. Setting appropriate double gates in the n-$\gamma\gamma\gamma$ cubes obtained from the present experiments we could not establish any coincidence relation between the 1575.1- and the 1002.2-keV transition. Instead, a rotational-like cascade consisting of 1273.5- and 1389.8-keV lines [see Fig. 2(c)] extends the nonyrast structure built on the second

TABLE II. Angular distribution coefficients and mixing ratios in ^{69}Se from the ^{40}Ca(^{32}S,$2pn$)^{69}Se reaction at 105-MeV beam energy.

E_γ(keV)	$I_i^{\pi i} \rightarrow I_f^{\pi f}$	$A_2/A_0 \pm \Delta(A_2/A_0)$	$A_4/A_0 \pm \Delta(A_4/A_0)$	$\delta \pm \Delta\delta$
714.2	$23/2^- \rightarrow 19/2^-$	0.238 ± 0.06	-0.0807 ± 0.01	$-0.067^{+0.063}_{-0.073}$
598.2	$21/2^- \rightarrow 19/2^-$	-0.142 ± 0.04	-0.085 ± 0.03	0.05 ± 0.03
468.0	$19/2^- \rightarrow 15/2^-$	0.157 ± 0.05	-0.11 ± 0.07	-0.16 ± 0.06
448.2	$19/2^- \rightarrow 17/2^+$	0.245 ± 0.6	0.025 ± 0.01	0.32 ± 0.05[a]
412.0	$17/2^- \rightarrow 15/2^-$	-0.172 ± 0.05	-0.02 ± 0.01	0.50 ± 0.4
1130.2	$29/2^+ \rightarrow 25/2^+$	0.511 ± 0.04	0.007 ± 0.002	0.17 ± 0.4[b]
1182.3	$25/2^+ \rightarrow 21/2^+$	0.359 ± 0.03	-0.154 ± 0.06	0.0 ± 0.01
1079.1	$13/2^+ \rightarrow 9/2^+$	0.29 ± 0.03	-0.06 ± 0.03	0.0 ± 0.01
403.1	$13/2^+ \rightarrow 11/2^+$	0.005 ± 0.001	-0.0015 ± 0.0007	0.16 ± 0.05
773.3	$13/2^+ \rightarrow 11/2^+$	0.47 ± 0.1	0.105 ± 0.075	2.30 ± 0.39
				$0.57^{+0.10}_{-0.07}$
675.9	$11/2^+ \rightarrow 9/2^+$	0.35 ± 0.07	0.057 ± 0.02	$2.52^{+0.55}_{-0.44}$
				$0.57^{+0.10}_{-0.08}$

[a]Small contamination at backward angles with the 442.9-keV transition in ^{69}As.
[b]Small contamination at backward angles with the 1125.3-keV transition in ^{68}Ge.

$25/2^+$ state. We found the 1002.2-keV transition to feed the $21/2^+$ yrast state directly with a very low intensity which does not allow us to extract its DCO value and determine the spin of the level at 5257.9 keV. This level is populated by the 1219.4-keV transition which decays from the newly observed state at 6477.2-keV excitation energy.

The small difference between the energies of the γ rays in the high-spin part of the level scheme and those reported in

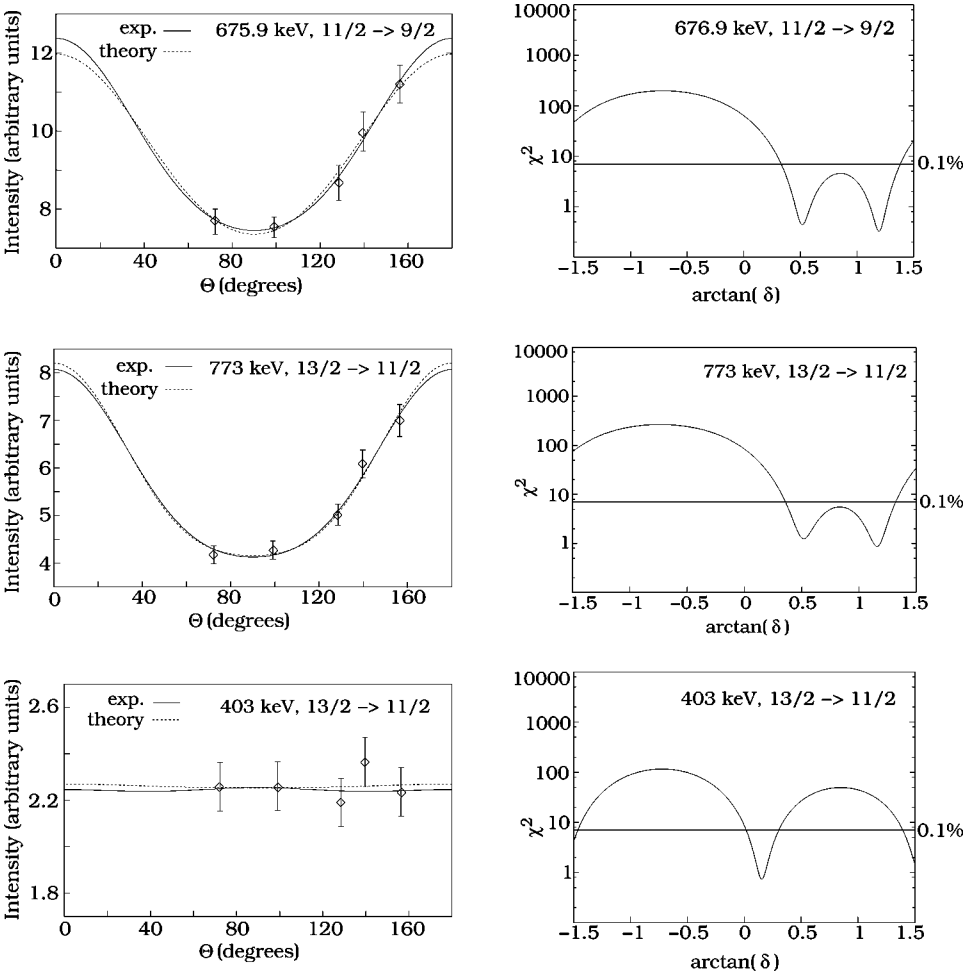

FIG. 3. Left: angular distribution data for the 675.9-, 773.2-, and 403.1-keV ^{69}Se γ rays. Right: plots of χ^2 vs the mixing ratio δ for the angular distribution of the respective γ rays. The initial- and final-spin states which were tested are indicated on the plots.

the previous work [19] may be the result of the low statistics and large Doppler broadenings of the peaks at high energies. The peak half-width at 1.3 MeV is about 10 keV in the experiment with the self-supporting target and about 2.6 keV in the experiment with the gold-backed ^{40}Ca target.

B. Negative-parity states

The first three negative-parity levels lie at very low excitation energies. The DCO values for the 129.1- and 161.3-keV transitions show their dipole and quadrupole character, respectively. While a $3/2^-$ value for the spin of the level at 129.1 keV was already assigned by Jenkins *et al.* [19], the systematics of nuclei with $N=35$ such as ^{63}Ni and ^{67}Ge suggest us the spin $3/2^-$ as well for the level at 290.1 keV. In general, the negative-parity part of the level scheme shows a large density of levels mostly concentrated below 3.5-MeV excitation energy. They were very strongly populated in the experiment using a thick target, and the small peak width characteristic of the experiments using thick targets made possible the disentanglement of the doublets, their placement in the level scheme with good accuracy in energy, and clean gates with good statistics in the DCO-ratio measurements. These states can be classified into two groups. The new levels at 1134.7, 2079.4, and 2979.6 keV, together with the levels at 1193.8 and 2618.1 keV found by Wiosna [3] and confirmed by Jenkins *et al.* [19] and in the present work are populated from the $17/2^-$ state at 3617.6 keV. The levels at 1123.5 and 2398.6 keV and the levels at 914.6 and 2433.9 keV are populated from the state at 3205.6 keV and they show similar spin sequences and energy spacings. The spin assignments for these levels were confirmed by the DCO ratios extracted in the present experiment. The γ rays depopulating the newly observed cascade consisting of 2979.6-, 2079.4-, 1134.7-, and 290.1-keV levels are clearly seen in the spectrum presented in Fig. 2(d). Based on DCO measurements, we assigned to these levels the spins $13/2^-$, $9/2^-$, $5/2^-$, and $3/2^-$, respectively. The $15/2^-$ and $19/2^-$ yrast states are fed by the $E2$ transitions of 468.0 and 714.2 keV, respectively, and by a parallel $M1/E2$ cascade via the 56.2−412.0-keV and 116.4−598.2-keV γ rays.

V. DISCUSSION

The strongly coupled like positive-parity structure which develops at low excitation energies in ^{69}Se obviously points to a large oblate deformation. Thus, the involved Nilsson configuration is the $K=9/2$ orbit of the $g_{9/2}$ orbital. In the limit of high-K orbitals near the Fermi surface, the Coriolis effects are minimal for the yrast states and they may resemble pure Nilsson states with a relatively pure K. The nonregular character of the rotational yrast band in ^{69}Se with the large signature splitting suggests a strong admixture with low-K orbits. This strong K mixing in the yrast band may be understood when taking into account the fact that the yrast band in ^{69}Se is the result of coupling the odd-neutron to the states of the ^{68}Se core. As we pointed out at the beginning of this paper, two bands with different deformations have been found to coexist at low spin in ^{68}Se—the oblate ground-state band and the prolate quasi-γ-band [10–12]. In ^{69}Se only one rotational band has been observed and its levels may contain contributions from both bands, one of them being dominant. The coexistence of two bands involves the mixing of the K values characterizing these bands. Thus, the oblate-prolate mixing of ^{68}Se is strongly reflected in the yrast structure in ^{69}Se whose states will also be characterized by mixed K values.

Since a rotational model treating an odd-particle coupled to a symmetric rotor deals only with well defined K values, we will try to describe the positive-parity one-quasiparticle states in ^{69}Se by applying the RTRP model. The model describes an odd system of nucleons by coupling a quasiparticle to a triaxial Davydov even-even core [36]. Within this model, the shape of the nucleus is defined by two deformation parameters, namely, the quadrupole deformation ϵ_2 and the asymmetry parameter γ. These parameters are kept fixed throughout the calculation (rigid rotor). The values $\gamma=0°$, 60° correspond to the prolate and oblate axial symmetrical cases, respectively. In the RTRP model, the K mixing discussed above depends directly on the asymmetry parameter γ. Besides the energies and the signature splitting of the positive-parity yrast states, we will also examine how well their electromagnetic properties and the properties of the observed yrare levels can be described assuming a rigid triaxial shape for ^{69}Se.

A. The model

The RTRP model is described in detail in the original paper of Larsson, Leander, and Ragnarsson [14]. A particle couples to a rigid rotor so that the Hamiltonian of the odd system can be written as

$$H = H_{sp} + H_{pair} + H_{core}. \tag{2}$$

The single-particle Hamiltonian H_{sp} describes the odd particle in a deformed modified oscillator potential characterized by the deformation parameters ϵ_2 and γ. The parameters for the modified oscillator potential are those of Bengtsson and Ragnarsson [37]. H_{pair} represents the pairing force acting between like nucleons and is included in the model by a standard BCS calculation. The Fermi level and the pairing gap are derived quantities and not adjustable parameters.

The core Hamiltonian has the typical form

$$H_{core} = \sum_{\kappa=1}^{3} \frac{(I_\kappa - j_\kappa)^2}{2\Im_\kappa}, \tag{3}$$

where I and j are the total and particle angular momenta, respectively. The moments of inertia $\Im_\kappa$ are assumed to be of hydrodynamical type

$$\Im_\kappa = \frac{4}{3}\Im_0 \sin^2\left(\gamma + \frac{2\pi}{3}\kappa\right). \tag{4}$$

The fixed moment of inertia $\Im_0$ can be derived from the core excitation energy $E(2^+)$. The codes employed in this work [38–40] allow also calculations with a variable moment of inertia [41], but in order to reduce the number of the free

parameters, we used only a constant moment of inertia. The strong-coupling basis is used for the diagonalization of the particle-rotor Hamiltonian

$$|IMK\nu\rangle = \sqrt{\frac{2I+1}{16\pi^2}} \sum_{Nlj\Omega} c^{(\nu)}_{Nlj\Omega}[D^I_{MK}|Nlj\Omega\rangle + (-1)^{I+K} D^I_{M-K}|Nlj-\Omega\rangle]. \quad (5)$$

The symbol ν labels the different deformed single-particle states. Up to 15 single-particle orbitals can be included in the calculations. The strong-coupling basis states of the complete system $|IMK\nu\rangle$ are labeled by the projection K of I on the intrinsic axis 3 (quantization axis); due to triaxiality, the relation $K=\Omega$ is not longer valid.

The agreement between the experimental and calculated spectra can be improved by introducing an additional parameter ξ—the Coriolis attenuation parameter which multiplies the matrix elements of the Coriolis term in the Hamiltonian.

B. RTRP description of the low-lying positive-parity states in ^{69}Se

The main fit parameters of the model are the deformation parameters β and γ and the energy of the first excited core state $E(2^+)$. These parameters have been fitted to the excitation energies and to several important branching ratios. We started the calculations for the yrast positive-parity band by considering values for the quadrupole deformation in the range $0.25 \leqslant \epsilon_2 \leqslant 0.35$ as suggested by the systematics of the odd-A selenium isotopes. Of course, values outside this range have not been excluded from the fit either. In the calculations, $g_{9/2}$, $g_{7/2}$, and $d_{5/2}$ single-particle orbitals have been considered. The best agreement with the experimental data has been obtained for $\epsilon_2=0.33$. This value agrees with the deformation $\beta_2=-0.32$ for the ground-state band in the even-even core ^{68}Se derived by Petrovici *et al.* [12] from complex EXCITED VAMPIR [42] calculations. We have to point out that the parameters given in the results of the fit respect the "Copenhagen convention," according to which the asymmetry parameter γ takes values in the range 0° (prolate shape) to 60° (oblate shapes) with positive values for the quadrupole deformation, ϵ_2.

The obtained fitted value for core excitation energy is $E(2^+)=500$ keV, smaller than the experimental energy of 854 keV of the first 2^+ state in ^{68}Se. A fitted value $E(2^+)=230$ keV was reported by Jenkins *et al.* [43] in their two quasiparticle-rotor model calculations performed for the odd-odd nucleus ^{70}Br, with the two quasiparticles being a proton and a neutron in the $g_{9/2}$ shell. The inconsistencies between the experimental and the calculated $E(2^+)$ values were associated, in Ref. [43], with the shape coexistence of ^{68}Se. Besides, one should always take into account the fact that the model treats the coupling to an even-even core of a quasiparticle, e.g., a mixture of a particle and a hole state. Therefore, one cannot expect to obtain agreement between experiment and theory when choosing the value of $E(2^+)$ parameter just equal to the energy of the first excited state in the ^{68}Se or ^{70}Se nuclei.

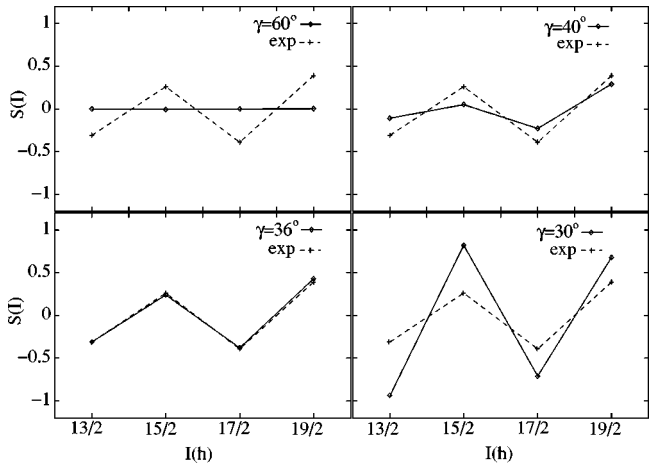

FIG. 4. Experimental and calculated signature splitting for the one-quassiparticle states of the positive-parity yrast band in ^{69}Se. The RTRP parameters used in the calculations are given in Table III.

The optimal value of the asymmetry parameter is found from the signature splitting which is very sensitive to any variation of γ. A measure of the signature splitting is the expression [44]

$$S(I) = \frac{E(I)-E(I-1)}{E(I)-E(I-2)} \frac{I(I+1)-(I-2)(I-1)}{I(I+1)-I(I-1)} - 1. \quad (6)$$

A vanishing splitting (pure rotor spectrum, strong coupling) corresponds to the value $S(I)=0$. Figure 4 displays both the theoretical and experimental functions for the spin sequence of the yrast levels. The observed signature splitting cannot be reproduced with an axial oblate shape ($\gamma=60°, \epsilon_2>0$). Varying γ between 60° and 40° will produce only small changes in the theoretical function, but the changes become important when γ approaches the maximum triaxiality where $\gamma=36°$ reproduces very well the experimental splitting.

Only a small attenuation of the Coriolis force was necessary and the optimum results were obtained for $\xi=0.95$. The model parameters used in the present calculations are given in Table III.

The comparison of the experimental and calculated energy levels of ^{69}Se is shown in Fig. 5. The calculations provide the four low-lying positive-parity band structures which have been observed experimentally. The calculated levels are normalized to the experimental energy of the bandhead with

TABLE III. The RTRP parameters used in the present work: quadrupole deformation ϵ_2, asymmetry parameter γ, core 2^+ state energy, and Coriolis attenuation factor ξ. κ_n and μ_n are the Nilsson parameters for neutrons in the $N=4$ oscillator shell, taken from Ref. [37].

ϵ_2	γ (deg)	$E(2^+)$ (MeV)	ξ	κ_n	μ_n
^{69}Se, $\pi=+0.33$	36°	0.5	0.95	0.070	0.39

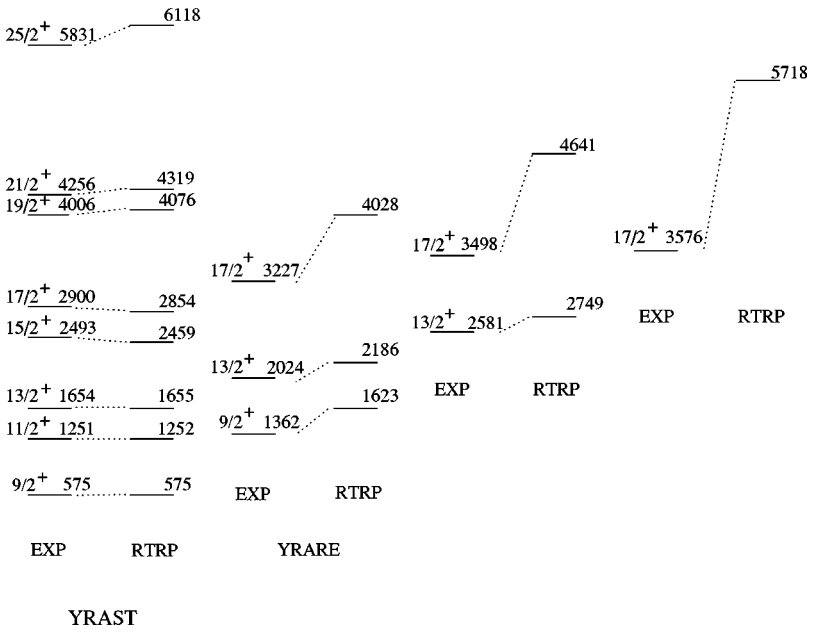

FIG. 5. Experimental and calculated positive-parity levels in ^{69}Se. The RTRP parameters used in the calculations are given in Table III.

spin $9/2^+$. In Fig. 5 only the theoretical levels which have an experimental partner were represented. The set of parameters which describes very well the experimental signature splitting (Table III) can successfully reproduce the experimental energies of the one-quasiparticle yrast positive-parity states. The other nonyrast levels, especially the $17/2^+$ states, are predicted by the model higher in energy. The calculated levels are dominated by the $g_{9/2}$ single-particle orbital which gives a contribution of $\sim$80 % to the total wave function of the yrast and yrare states. The $d_{5/2}$ and $g_{7/2}$ orbitals contribute only with small amplitudes (see Table IV). The amplitudes of the core states in the total wave functions are presented in Fig. 6. The $2_2^+, 3^+, 4_2^+, \ldots$ core states form the quasi-γ-band of a triaxial rotor; there is no β band of the core in this model. The wave functions associated to the yrast calculated levels reveal the probability that the core in the ground band is larger than 90° (Fig. 6, top). The nonyrast calculated levels contain an increased contribution from the quasi-γ-band states of the core (Fig. 6, bottom). The quasi-γ-band in ^{68}Se was experimentally and theoretically found to have a prolate character with a slightly different quadrupole deformation with respect to the ground-state band. Thus, the nonyrast states may be reproduced with a different set of deformation parameters ϵ_2 or/and γ. The restriction to a rigid rotor core employed by the model is a limitation in the study of these states.

TABLE IV. Relative single-particle structure of positive-parity states in ^{69}Se calculated with the RTRP model (parameters $\epsilon_2 = 0.33$, $\gamma = 36°$ and see Table III). For each spin the squared amplitude is given for the yrast and yrare states.

	Yrast states			Yrare states		
Spin	$g_{9/2}$	$d_{5/2}$	$g_{7/2}$	$g_{9/2}$	$d_{5/2}$	$g_{7/2}$
$9/2^+$	88.44	9.94	0.7	79.8	14.4	2.75
$11/2^+$	87.0	10.6	1.03			
$13/2^+$	84.9	11.6	1.66	85.7	11.3	1.3
$15/2^+$	58.9	11.1	1.4			
$17/2^+$	80.8	13.4	2.9	84.3	12.2	1.5
$19/2^+$	84.2	11.9	1.9			
$21/2^+$	78.7	14.2	3.6			
$23/2^+$	82.8	12.5	2.4			
$25/2^+$	77.5	14.6	4.2			

The model predicts a $25/2^+$ state at an excitation energy of $E_x = 6118$ keV which may correspond to the experimental state at 5830.8 keV. In this case, the level at 5830.8 keV could be regarded as the continuation of the oblate band.

Figure 7 shows a comparison between the experimental and the calculated branching ratios for the yrast and yrare states using the relation

$$\lambda = \left(\frac{T(M1; I \to I-1) + T(E2; I \to I-1)}{T(E2; I \to I-2)} \right)_{RTRP} = \frac{I_\gamma(I \to I-1)}{I_\gamma(I \to I-2)}. \quad (7)$$

The given ratios for the yrare levels are extracted between the in-band $I \to I-2$ transition and the corresponding $I \to I-1$ transition populating the levels of the yrast band. The intensity ratio $I_\gamma(I \to I-1)/I_\gamma(I \to I-2)$ for the decay of a given state I has been determined in the most direct way, namely, from the coincidence spectrum with a gate on the in-band transition populating the state under investigation.

The theoretical branching ratios represented in Fig. 7 were calculated using the model parameters given in Table III. In the evaluation of the electromagnetic moments, an effective g_s factor of 0.7 g_s^{free} has been used and g_R has been taken as the ratio $Z/A = 0.492$. For the sake of comparison, the calculated branching ratios assuming an axial oblate shape ($\gamma = 60°$) are also represented in the plots. For both yrast and yrare structures, the experimental ratios are better reproduced when assuming a rigid triaxial shape. Calcula-

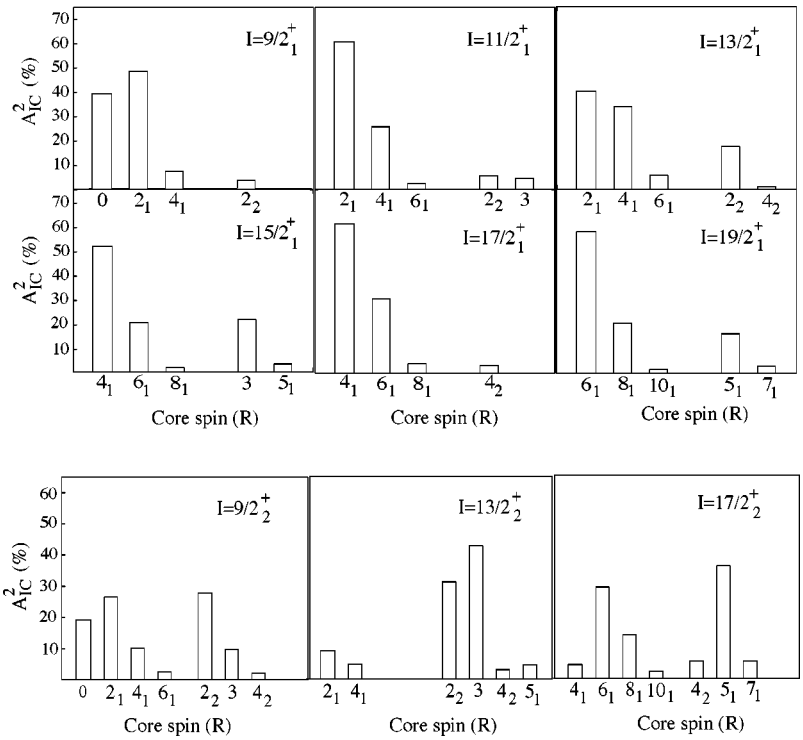

FIG. 6. Squared amplitudes A^2_{IC} of core states for positive-parity yrast (top) and yrare (bottom) bands of ^{69}Se calculated with the RTRP model. The model parameters used in the calculations are given in Table III.

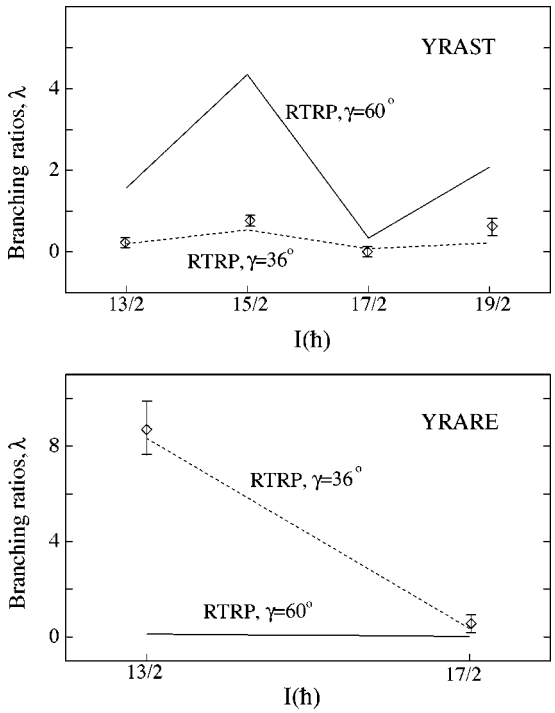

FIG. 7. Experimental branching ratios (points) compared to the calculated values using the RTRP model for $\gamma=36°$ (dotted lines) and $\gamma=60°$ (oblate axial symmetric) (solid lines). The theoretical values are based on calculated matrix elements and experimental γ-ray energies. The RTRP model parameters are those given in Table III.

tions with an axial oblate shape predict branching ratios which are larger than the measured ones for the yrast states. The calculations with $\gamma=36°$ predict a small $B(E2)$ value for the in-band $13/2^+_2 \rightarrow 9/2^+_2$ transition, thus reproducing the observed enhancement of the out-of-band $13/2^+_2 \rightarrow 11/2^+_1$ decay. However, the RTRP results for the yrare band should be regarded with some precaution because due to the shape-coexistence phenomenon, the rigid core approximation assumed for the shape of the ^{69}Se nucleus may not be valid for these states.

The determination of the absolute $B(M1)$ and $B(E2)$ reduced transition probabilities requires the measurement of the nuclear lifetimes and mixing ratios of the levels and transitions involved. However, no lifetimes were determined in the present work and only the mixing ratios of the $13/2^+_1 \rightarrow 11/2^+_1$, 403.1-keV and $13/2^+_2 \rightarrow 11/2^+_1$, 773.3-keV transitions could be determined. One can thus compare the theoretical and the experimental ratios between the in-band $B(M1;I \rightarrow I-1)$and the $B(E2;I \rightarrow I-2)$ values of the 403.1- and 1079.1-keV transitions depopulating the $13/2^+$ yrast level at 1653.7-keV excitation energy and the ratios between the out-of-band $B(M1;I \rightarrow I-1)$ value to the in-band $B(E2;I \rightarrow I-2)$ value of the 773.3- and 662.3-keV transitions depopulating the $13/2^+$ yrare level at 2023.8-keV excitation energy. The ratios of reduced transition probabilities are given in Table V; the experimental ratios have been calculated using the equation

$$\frac{B(M1;I \rightarrow I-1)}{B(E2;I \rightarrow I-2)} = 0.6967 \frac{E^5_\gamma(I \rightarrow I-2)}{E^3_\gamma(I \rightarrow I-1)} \frac{\lambda}{(1+\delta^2)} \quad \mu^2_N/e^2\ \mathrm{b}^2. \tag{8}$$

The γ-ray energies E_γ are given in MeV, λ is the measured branching ratio extracted by applying the second part of Eq.

TABLE V. Experimental and theoretical values of the mixing ratios δ, branching ratios λ, and $B(M1)/B(E2)$ ratios in ^{69}Se.

		Experiment			RTRP, $\gamma=36°$		
$I_i \rightarrow I_f$	E_γ (keV)	λ	δ	$B(M1)/B(E2)$ $(\mu_N/e\ \mathrm{b})^2$	λ	δ	$B(M1)/B(E2)$ $(\mu_N/e\ \mathrm{b})^2$
$13/2^+_1 \rightarrow 11/2^+_1$	403	0.18(2)	0.16±0.05	2.7(12)	0.20	0.12	3.06
$13/2^+_1 \rightarrow 9/2^+_1$	1079						
$13/2^+_2 \rightarrow 11/2^+_1$	773	8.7(7)	2.30±0.39	0.25(9)	8.34	0.71	1.18
$13/2^+_2 \rightarrow 9/2^+_2$	662						

(7), and δ is the $E2/M1$ mixing ratio. The RTRP model reproduces very well the observed electromagnetic properties of the transitions depopulating the $13/2^+$ yrast state and predicts a value of 0.12 for the mixing ratio of the 403.1-keV transition.

In general, the one-quasiparticle yrast positive-parity states in ^{69}Se and their properties can be well reproduced in the framework of rigid triaxial rotor plus particle model. The fit of the experimental signature splitting and branching ratios demonstrates the importance of a nonaxial symmetry calculation. More experimental data, in particular lifetime measurements in the one-quasiparticle bands, would be helpful for a more complete description of the shape of this nucleus.

C. Three quasiparticle positive-parity bands

Figure 8 shows the kinematic moments of inertia of the oblate yrast and the excited configurations in ^{68,69}Se. Also shown are the kinematic moments of inertia of the oblate ground-state band, the neutron aligned and the proton aligned bands in ^{68}Ge [45,46]. Please note the similarity between the behavior of the moment of inertia of the excited prolate configurations in ^{69}Se and ^{68}Ge.

The aligned angular momentum $i_x(i_x=I_x-i_{ref})$ for the oblate bands (top) and the excited prolate configurations (bottom) for all three nuclei are presented in Fig. 9. Two K values are used in the calculation of the alignments in ^{69}Se since for triaxial deformation the K value is not well defined. A K=0.5 value corresponds to prolate deformation while K =4.5 corresponds to oblate deformation. The difference in initial alignment at low rotational frequencies $[i(\omega)\approx 4\hbar]$ with respect to the even-even ^{68}Se and ^{68}Ge nuclei implies a nearly complete alignment of the odd neutron in a $g_{9/2}$ orbital with the axis of rotation. The sharp backbend at the rotational frequency $\hbar\omega\approx 0.6$ MeV and the gain in alignment of $\sim 7\hbar$ units of angular momentum are consistent with the alignment of a pair of $g_{9/2}$ protons occupying the low 1/2 [440] orbital at prolate deformation. This indicates a strong polarization of the core and shape change in ^{69}Se from oblate triaxial shape at low spin to prolate shapes at intermediate spin. The observed similarity between the backbends and the alignments of the excited structure in ^{69}Se and the proton-aligned configuration in ^{68}Ge reciprocally confirms their nature and suggests a similarity in the shape of the two nuclei in this spin region. A second crossing occurs in both nuclei in the frequency range $\hbar\omega=0.8-0.9$ MeV. They look again similar and they may have the same character. Theoretically, a neutron alignment may take place but a second proton alignment cannot be excluded.

D. Negative-parity bands

At low energies, the negative-parity states in ^{69}Se do not show a rotational structure as observed in the heavier odd-Se and Br isotopes, suggesting a smaller deformation for this part of the level scheme and possibly predominant shell model characteristics. Negative-parity decoupled rotational bands develop already at very low excitation energies in ^{71}Se [47] and ^{71,73}Br nuclei [48,49]. With increasing the neutron

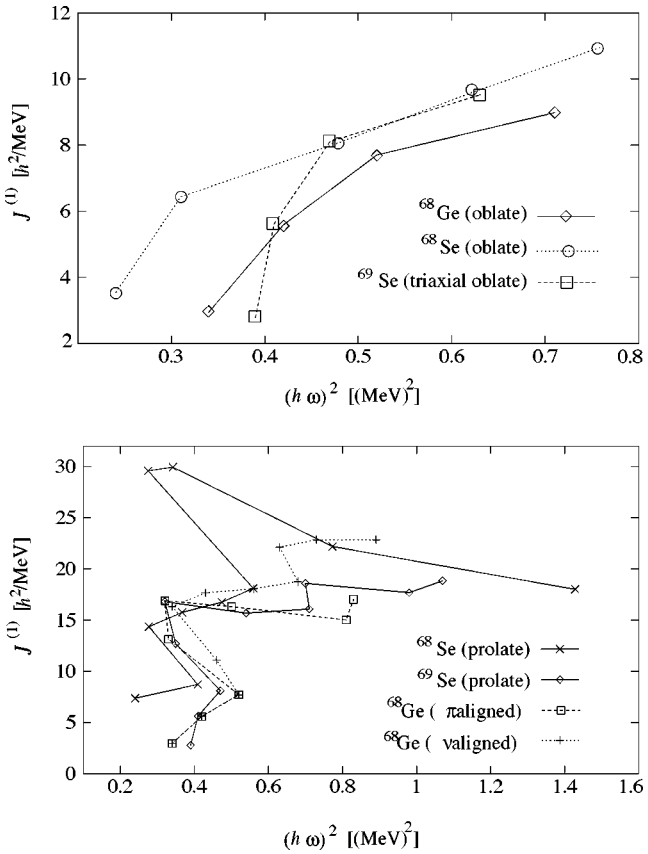

FIG. 8. Experimental kinematic moments of inertia $\mathfrak{I}^{(1)}$ for the oblate ground-state structures (top) and the excited prolate configurations (bottom) in ^{68,69}Se and ^{68}Ge.

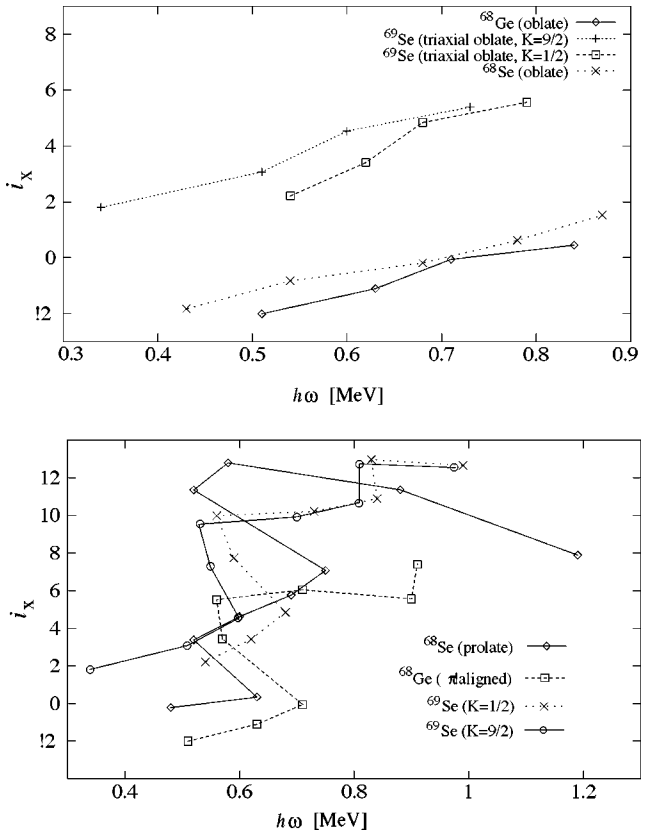

FIG. 9. Experimental alignments i_x for the oblate ground-state structures (top) and the excited prolate configurations (bottom) in ^{68,69}Se and ^{68}Ge. Harris reference parameters $\Im_0 = 6.0\hbar^2$ MeV^{-1} and $\Im_0 = 3.5\hbar^4$ MeV^{-3} have been used for all nuclei.

number, strongly-coupled negative-parity structures characterize the ^{73,75,77}Se [50–52] and ^{75,77}Br isotopes [53,54]. Thus, at low excitation energies, the negative-parity structure of ^{69}Se fits better in the systematics of neighboring odd-Ge isotopes, whose structural and electromagnetic properties at low excitations are due to both neutron and proton shell effects and to small shape deformations connected with the departure from closed shells, defining a transitional region where neither shell nor collective effects can be expected to predominate.

In order to determine whether the low-lying excitations of ^{69}Se are mainly shell excitations or mainly collective modes, one needs complete experimental information about the level scheme and electromagnetic properties. Because the experimental information is still far from complete we discuss here only qualitatively the negative-parity bands found in ^{69}Se.

The energy spacing and sequence of spins $\left(\frac{1}{2}^-, \frac{5}{2}^-, \frac{3}{2}^-, \frac{3}{2}^-\right)$ of the ground state and the first three excited negative-parity states in ^{69}Se follow the pattern observed in the $N=35$ nuclei, ^{63}Se, ^{65}Zn, and ^{67}Ge in the mass region [18,56,57]. These levels were generally interpreted as being generated by single-particle excitations of the odd neutron lying in the $p_{3/2}$, $f_{5/2}$, and $p_{1/2}$ negative-parity shells.

Above spin $15/2^-$ and excitation energies around 3 MeV, the collective excitations predominate. The $15/2^-$ state at 3206 keV is the only certain candidate for the octupole state in ^{69}Se. Making use of our angular correlation and distribution results, no other $15/2^-$ states were identified. The states $15/2^-$, $19/2^-$, and $23/2^-$ at 3205.6-, 3673.6-, and 4387.8-keV excitation energies may be interpreted as the $g_{9/2}$ particle or hole coupled to the 3^-, 5^-, and 7^- states in the neighboring even-even nuclei ^{68,70}Se [10,55]. Such a coupling picture follows the trend observed within the chain of Ge isotopes between ^{64}Ge and ^{70}Ge which suggested their interpretation in the framework of the weak-coupling model [31,33]. The energies of these states agree very well with the energies of the corresponding core states in ^{70}Se, while the tentatively assigned analogous states in ^{68}Se are about 200–300 keV higher in energy. The occurrence of the two coexisting parallel structures (bands 6 and 7 in Fig. 1) starting at a tentative spin of $(29/2^-)$ suggests a change in structure at high spin [19].

VI. SUMMARY

We have revised and extended the previously known level scheme for the $N=Z+1$ nucleus ^{69}Se employing the ^{40}Ca(^{32}S,2pn) reaction. Double and triple γ-ray coincidences gated with particles, as well as angular distributions and directional correlations, have been measured. The $19/2^+$ state belonging to the oblate yrast band has been established at $E_x \sim 4$ MeV. Above this energy, the oblate structure is crossed by a prolate configuration whose kinematic moment of inertia and alignment show the same characteristics as those in the even-even ^{68}Ge nucleus. An important aspect for future work will be the determination of the deformation of these nuclei in the band-crossing region.

The low-lying negative-parity states appear to be consistent with the systematics of $N=35$ isotones, suggesting a small deformation and predominant shell model characteristics for this part of the level scheme. Above $E_x \sim 3$ MeV excitation energy the collective excitations become important.

The one-quasiparticle states of the yrast and near yrast positive-parity bands have been discussed in terms of a particle coupled to a rigid triaxial rotor model. The model reproduces very well the properties of the yrast states such as the signature splitting, excitation energies, and branching ratios, but only if a substantial deviation from axial symmetry is taken into account. The rigid shape assumed for the core represents, of course, a limitation and γ must be regarded as an effective parameter. We can conclude that one quasiparticle coupled to a rigid triaxial core is able to explain the main characteristics of the low-lying levels in ^{69}Se.

ACKNOWLEDGMENTS

One of the authors (I.S.) thanks Dr. P. Petkov and Dr. A. Lisetskiy for useful discussions. A. J. acknowledges financial support from the Deutsche Forschungsgemeinshaft (DPG) within the Heisenberg program. The authors thank the crew of the VIVITRON accelerator for their efficient support during the experiments. The authors would like to thank Professor I. Ragnarsson and P. Semms for kindly providing the computer codes for triaxial nuclei. This work was supported by BMBF under Contract Nos. 06 OK 958 and 06 GÖ 951 and the EUROVIV Contract No. HPRI-CT-1999-000783.

[1] C. J. Lister, B. J. Varley, H. G. Price, and J .W. Olness, Phys. Rev. Lett. **49**, 308 (1982).
[2] T. Mylaeus *et al.*, J. Phys. G **15**, L135 (1989).
[3] M. Wiosna *et al.*, Phys. Lett. B **200**, 255 (1988).
[4] S. Skoda *et al.*, Z. Phys. A **336**, 391 (1990).
[5] S. Freund *et al.*, Phys. Lett. B **302**, 167 (1993).
[6] W. Nazarewicz, J. Dudek, R. Bengtsson, T. Bengtsson, and I. Ragnarsson, Nucl. Phys. **A435**, 397 (1985).
[7] A. Petrovici, K. W. Schmid, F. Grümmer, and A. Faessler, Nucl. Phys. **A517**, 108 (1990).
[8] D. Sohler *et al.*, Nucl. Phys. **A644**, 141 (1998).
[9] J. H. Hamilton *et al.*, Phys. Rev. Lett. **32**, 239 (1974).
[10] S. M. Fischer *et al.*, Phys. Rev. Lett. **84**, 4064 (2000).
[11] S. M. Fischer, C. J. Lister, and D. P. Balamuth, Phys. Rev. C **67**, 064318 (2003).
[12] A. Petrovici, K. W. Schmid, and A. Faessler, Nucl. Phys. **A710**, 246 (2002).
[13] J. Heese *et al.*, Z. Phys. A **325**, 45 (1986).
[14] S. E. Larsson, G. Leander, and I. Ragnarsson, Nucl. Phys. **A307**, 189 (1978).
[15] J. A. Macdonald *et al.*, Nucl. Phys. **A288**, 1 (1977).
[16] M. Ramdane *et al.*, Phys. Rev. C **37**, 645 (1988).
[17] J. W. Arrison *et al.*, Phys. Rev. C **40**, 2010 (1989).
[18] K. R. Pohl, D. F. Winchell, J. W. Arrison, and D. P. Balamuth, Phys. Rev. C **51**, 519 (1995).
[19] D. G. Jenkins *et al.*, Phys. Rev. C **64**, 064311 (2001).
[20] F. A. Beck, Prog. Part. Nucl. Phys. **28**, 443 (1992).
[21] J. Simpson, Z. Phys. A **358**, 39 (1997).
[22] J. Eberth *et al.*, Prog. Part. Nucl. Phys. **28**, 495 (1992).
[23] G. Duchêne *et al.*, Nucl. Instrum. Methods Phys. Res. A **432**, 90 (1999).
[24] A. Gadea *et al.*, LNL Annual Report No. 160/00, 1999, p. 151.
[25] Ö. Skeppstedt *et al.*, Nucl. Instrum. Methods Phys. Res. A **421**, 531 (1999).
[26] F. Pühlhofer, Nucl. Phys. **A280**, 267 (1977).
[27] D. Bazzacco (private communication).
[28] D. C. Radford, Nucl. Instrum. Methods Phys. Res. A **361**, 297 (1995).
[29] A. Krämer-Flecken *et al.*, Nucl. Instrum. Methods Phys. Res. A **275**, 333 (1989).
[30] D. Weil *et al.*, Nucl. Phys. **A567**, 431 (1994).
[31] U. Hermkens *et al.*, Phys. Rev. C **52**, 1783 (1995).
[32] U. Hermkens *et al.*, Z. Phys. A **343**, 371 (1992).
[33] F. Becker *et al.*, Nucl. Phys. **A626**, 799 (1997).
[34] S. Skoda *et al.*, Nucl. Phys. **A633**, 565 (1998).
[35] V. Zobel, L. Cleemann, J. Eberth, T. Heck, and W. Neumann, Nucl. Phys. **A346**, 510 (1980).
[36] A. S. Davydov and G. F. Filippov, Nucl. Phys. **8**, 237 (1958).
[37] T. Bengtsson and I. Ragnarsson, Nucl. Phys. **A436**, 14 (1985).
[38] I. Ragnarsson and P. Seems (private communication).
[39] I. Ragnarsson and P. Seems (private communication).
[40] I. Ragnarsson and P. Seems (private communication).
[41] H. Toki and A. Faessler, Nucl. Phys. **A253**, 231 (1975).
[42] A. Petrovici, K. W. Schmid, and A. Faessler, Nucl. Phys. **A605**, 290 (1996).
[43] D. G. Jenkins *et al.*, Phys. Rev. C **65**, 064307 (2002).
[44] N. V. Zamfir and R. Casten, Phys. Lett. B **260**, 265 (1991).
[45] A. P de Lima *et al.*, Phys. Rev. C **23**, 213 (1981).
[46] A. Petrovici, K. W. Schmid, F. Grümmer, and A. Faessler, Nucl. Phys. **A504**, 277 (1989).
[47] J. Eberth, L. Cleeman, and N. Schmal, in Proceedings of the International Symposium on In-Beam Nuclear Spectroscopy, Debrecen, Hungary, 1984, edited by Zs. Dombradi and T. Fenyes, 1984, p. 23.
[48] J. W. Arrison, T. Chapuran, U. J. Hüttmeier, and D. P. Balamuth, Phys. Lett. B **248**, 39 (1990).
[49] S. Wen *et al.*, J. Phys. G **11**, L173 (1985).
[50] F. Seifert *et al.*, Z. Phys. A **430**, 141 (1991).
[51] G. D. Johns, J. Döring, R. A. Kaye, G. N. Sylvan, and L. S. Tabor, Phys. Rev. C **55**, 1175 (1997).
[52] G. Z. Solomon, G. D. Johns, R. A. Kaye, and L. S. Tabor, Phys. Rev. C **59**, 1175 (1999).
[53] A. J. Kreiner *et al.*, Phys. Rev. C **24**, 148 (1981).
[54] J. Döring, L. Funke, R. Schwengner, and G. Winter, Phys. Rev. C **48**, 2524 (1993).
[55] G. Rainovksi *et al.*, J. Phys. G **28**, 2617 (2002).
[56] M. J. Murphy, C. N. Davids, E. B. Norman, and R. C. Pardo, Phys. Rev. C **17**, 1574 (1978).
[57] M. J. Murphy and C. N. Davids, Phys. Rev. C **28**, 1069 (1983).
[58] R. B. Firestone, *Table of Isotopes*, 8th ed. (Wiley, New York, 1998).